

COMPOSITE MATERIALS UNDER TRANSVERSE BIAXIAL LOADS: STUDY OF THE INFLUENCE OF A NEARBY FIBRE ON THE INTERFACE CRACK GROWTH UNDER TENSION

C. Sandino¹, E. Correa² and F. París

Elasticity and Strength of Materials Group, School of Engineering, University of Seville,
Camino de los Descubrimientos s/n, 41092 Seville, Spain.

¹csandino@us.es ²ecorrea@us.es

Keywords: Micromechanics, Interfacial Fracture Mechanics, Matrix/inter-fibre failure, Two-fibre model, BEM.

Abstract

In this paper the interface crack growth associated with the inter-fibre failure under biaxial tension is studied by means of a two-fibre BEM model. A secondary transverse load, perpendicular to the transverse tension nominally responsible for the failure, is applied. The influence of the presence of an undamaged secondary fibre on the evolution of the interface crack at a primary one is analysed using Interfacial Fracture Mechanics concepts. When the secondary load is lower than or equal to one half of the principal load, the presence of the nearby fibre (for most of its positions) intensifies the inhibition of the mechanism of failure for biaxial tensile loads explained by the authors in previous studies. This tendency is not maintained when the nearby fibre is approximately aligned with the direction of the principal load, the presence of the fibre involving an accelerative effect versus failure. Nevertheless, for higher levels of the secondary load, the intensification of the inhibition of failure is detected for the whole range of positions of the secondary fibre under consideration.

1. Introduction

The analysis of the damage mechanism known as matrix/inter-fibre failure (occurring in fibrous composite materials submitted to loads perpendicular to the direction of the fibres) has already been the object of several studies conducted by the authors for the single-fibre [1-5] and the two-fibre cases [6, 7], considering different external loads.

In previous studies concerning uniaxial tension [1-5], the hypothesis that transverse failure starts with small debonds along the fibre-matrix interface was assumed. The position of these initial debonds is aligned with the direction of the external load, where the maximum values of the radial stress are detected. Then, the crack grows unstably along the interfaces until a certain crack length (60°-70°), coinciding with the appearance of a physically relevant contact zone at the crack tip. From that moment onwards, the interface crack grows in a stable way, favouring the kinking towards the matrix. The coalescence between different cracks in the matrix will eventually lead to the final macro-failure.

In this paper, the two-fibre BEM model employed in [6] is revisited to analyse the biaxial tensile problem. The influence of an undamaged secondary fibre on the interface crack that grows at a primary one is analysed, following the approach previously employed by the authors for uniaxial load [6]. While considering different positions of the undamaged fibre and different values of the secondary tensile load, the alterations brought about by the nearby fibre on the second stage of the matrix/inter-fibre failure are compared with respect to the results of a single-fibre model. The study is focused on crack morphology and propagation, and the results obtained are analysed by using Interfacial Fracture Mechanics concepts [8].

2. Numerical model

The numerical study was carried out using a tool based on BEM [9], and developed in [10]. This BEM code allows the numerical analysis of plane elastic problems for contact and interface cracks to be performed. The model employed is shown in Fig. 1 and represents the case of a crack which, under the plane strain hypothesis, grows along the interface in the presence of a nearby fibre. The appearance of the first debond is assumed to be associated with the direction of the principal load for all cases under consideration. In order to ensure the symmetry of crack growth with reference to the x-axis and for the purpose of making a comparison with the biaxial single-fibre case [5] and the uniaxial two-fibre case [6], a symmetrical model is established. Thus, the presence of the secondary fibre does not produce different effects at both crack tips. Notice that now the entire model consists of three fibres.

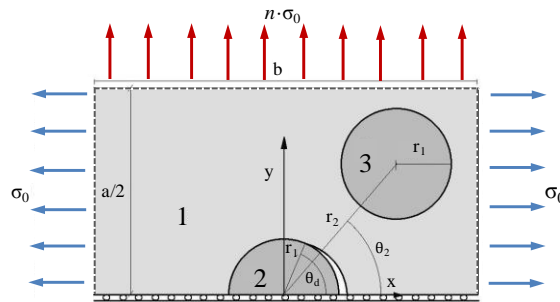


Figure 1. Model including a primary fibre with interface crack and an undamaged secondary fibre.

Solid 1 represents the matrix and Solids 2 and 3 the primary and secondary fibres respectively. The fibres' size is defined by the radius r_1 ($r_1=7.5 \cdot 10^{-6}$ m) whereas the matrix is large enough in order to avoid the border effect ($b=100 \cdot r_1$ and $a=b$). The position of the secondary fibre, defined by parameters r_2 and θ_2 , is changed in order to generate the cases under consideration. For this study, the initial distance employed between the fibres is $r_2=r_2^0=2.416 \cdot r_1$.

The materials chosen for the analysis correspond to a glass fibre-epoxy matrix system, whose elastic properties are included in Table 1.

Table 1. Elastic properties of the bi-material system.

Material	Young modulus, E (Pa)	Poisson coefficient, ν
Matrix (epoxy)	$E^m=2.79 \cdot 10^9$	$\nu^m=0.33$
Fibre (glass)	$E^f=7.08 \cdot 10^{10}$	$\nu^f=0.22$

With regard to the loads applied, the different cases follow the notation T- n T, where the first T represents the transverse tension nominally responsible for the failure (σ_0 , aligned with x-axis) and the term n T corresponds to the secondary load (aligned with y-axis). The n values considered in this study are $n=0, 0.25, 0.5, 0.75, 1$.

To describe the problem from the Fracture Mechanics point of view the Energy Release Rate, G , is used. The expression employed, based on [11], for a circular crack that propagates from a certain debonding angle, θ_d , Fig. 1, to $\theta_d+\Delta\theta_d$ ($\Delta\theta_d \ll \theta_d$), is:

$$G(\theta_d, \Delta\theta_d) = \frac{1}{2\Delta\theta_d} \int_{\theta_d}^{\theta_d+\Delta\theta_d} [\sigma_{rr}(\theta_d + \theta) \Delta u_r(\theta_d - \Delta\theta_d + \theta) + \sigma_{r\theta}(\theta_d + \theta) \Delta u_\theta(\theta_d - \Delta\theta_d + \theta)] d\theta \quad (1)$$

where θ is the circumferential coordinate with reference to the x-axis. σ_{rr} and $\sigma_{r\theta}$ represent, respectively, radial and shear stresses along the interface, and Δu_r and Δu_θ represent the relative

displacements of the crack faces. Both modes of fracture, I (associated with σ_{rr}) and II (associated with $\sigma_{\theta\theta}$), are obviously considered in Eq. (1). For this study the value of $\Delta\theta_d$ employed is 0.5° .

Dimensionless results for G will be presented. These values are obtained, following [12, 13], by dividing the values of G by G_0 :

$$G_0 = \left((1 + \kappa^m) / 8\mu^m \right) \sigma_0^2 r_1 \pi \quad (2)$$

where $\kappa^m = 3 - 4\nu^m$ and μ^m is the shear modulus of the matrix.

3. Energy Release Rate

The Energy Release Rate, G , of a growing interface crack is calculated from Eq. (1) in order to characterise the problem from the Interface Fracture Mechanics point of view. Assuming an initial debond of $\theta_d = 10^\circ$, G was obtained for the single-fibre and the two-fibre cases, a debonding angle interval $10^\circ \leq \theta_d \leq 150^\circ$ and all the T- n T cases under consideration. With regard to the two-fibre case, it is important to remark that, for $n = 0, 0.25, 0.5$ and all positions of the secondary fibre, the analysis of the radial stresses along the interface guaranteed the appearance of the initial debond at a similar position to that of the single-fibre case. For $n = 0.75, 1$, the initial debond was not guaranteed to appear at that position for all θ_2 values. Nevertheless, in this study, the cases $n = 0.75, 1$ were also analysed in order to obtain a better understanding of the effects of a growing secondary transverse load.

The results obtained for the single-fibre case, presented in Fig. 2, obviously agree with those presented in [5] and were employed as a reference for all cases reproduced with the two-fibre case. As can be observed in Fig. 2a, for the cases T-0.25T and T-0.5T, the G level increases with reference to the uniaxial single-fibre case, whereas for T-0.75T and T-T (Fig. 2b), it tends to maintain the G level of the uniaxial single-fibre case. While observing the results from a qualitative point of view, Mode I contribution becomes more relevant as the level of the secondary transverse load increases, i.e. a higher level of G_I is found and the disappearance of mixed mode propagation is achieved at greater debonding angles, which produces a translation of the G maxima for T-0.75T and T-T. On the contrary and with regard to the G value associated to the first debond considered ($\theta_d = 10^\circ$), it decreases as the secondary load increases, therefore the propagation of the initial damage requires a higher level of external load to be applied, involving a protecting effect versus failure with reference to the uniaxial single-fibre case [5].

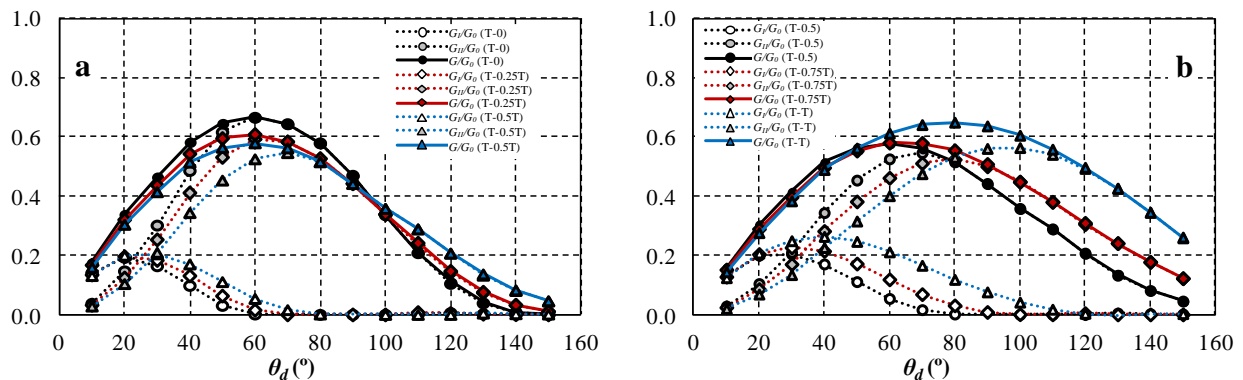


Figure 2. G/G_0 , G_I/G_0 and G_{II}/G_0 versus θ_d (single-fibre case): a) $n = 0, 0.25, 0.5$; b) $n = 0.5, 0.75, 1$.

The same approach was employed for the two-fibre case, calculating the G evolution for all the T- n T cases under consideration and a moving position of the secondary fibre ($r_2 = r_2^0$ and $25^\circ \leq \theta_2 \leq 155^\circ$). Fig. 3 represents these results for a selection of θ_2 values.

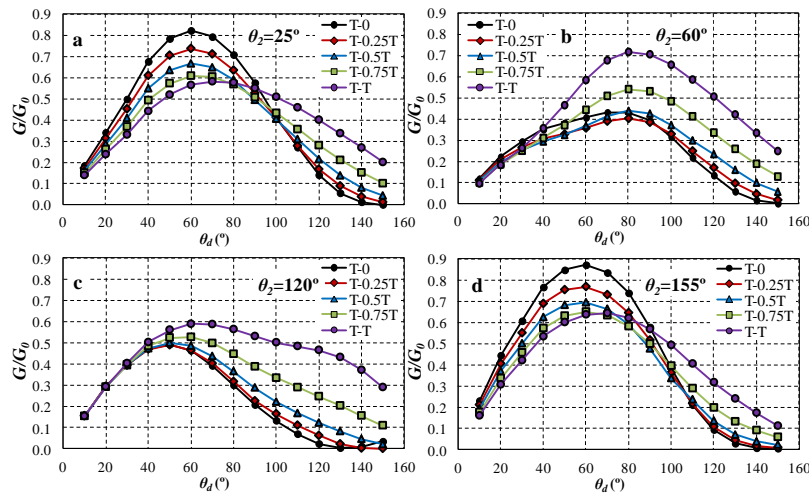


Figure 3. G/G_0 versus θ_d for $n=0, 0.25, 0.5, 0.75, 1$: a) $\theta_2=25^\circ$, b) $\theta_2=60^\circ$, c) $\theta_2=120^\circ$, d) $\theta_2=155^\circ$.

As can be observed in Figs. 3a and 3d, the G evolution for $\theta_2=25^\circ$ and $\theta_2=155^\circ$ (relative positions of the fibres approximately aligned with the direction of the principal load) presents the same tendency as the secondary load increases: G level decreases until the interface crack reaches $\theta_d \approx 80^\circ-100^\circ$ and increases from that debonding angle onwards. The intermediate positions present a difference tendency, as can be observed in Figs. 3b and 3c ($\theta_2=60^\circ$ and $\theta_2=120^\circ$): G level remains almost unaltered for $n=0, 0.25, 0.5$ and increases considerably for $n=0.75, 1$. In general, it is observed that as the secondary load increases, G evolutions for all positions of the secondary fibre tend to approach the G level of its corresponding single-fibre case (not represented in the figure), the effect of biaxial load becoming more important than the alterations brought about by the secondary fibre.

In order to evaluate the effect of the secondary fibre for the same value of the coefficient n and choosing $n=0.5$ as a representative case, Fig. 4 represents the evolution of G , G_I and G_{II} for a selection of positions of the secondary fibre, also including the curves associated with the $n=0$ and $n=0.5$ single-fibre cases. It can be observed that, when the relative positions of the fibres are approximately aligned with the direction of the principal load ($25^\circ \leq \theta_2 \leq 40^\circ$ and $140^\circ \leq \theta_2 \leq 155^\circ$), G values are total or partially above the single-fibre case evolution, whereas for the rest of the positions, G reaches lower values than the single-fibre case. This issue was also observed and explained in [6] for uniaxial tension, but the differences between the G evolutions with reference to the single-fibre case are less remarkable for the T-0.5T case.

Still observing Fig. 4 and regarding the G value associated with the first debond considered ($\theta_d=10^\circ$), it can be checked that it is lower than the single-fibre case value for most of the positions of the secondary fibre, intensifying the inhibition of the mechanism of failure provoked by the biaxial loading (previously commented in this section). This behaviour is not maintained for $140^\circ \leq \theta_2 \leq 155^\circ$: $G(\theta_d=10^\circ)$ is even above the uniaxial single-fibre case value (reference in this study), needing a lower level of load to initiate the propagation and, consequently, the presence of the fibre involving an accelerative effect versus failure. This tendency is also observed for the rest of the cases associated with $n \leq 0.5$, whereas for $n > 0.5$ the intensification of the inhibition of failure is detected for the whole range of positions of the secondary fibre under consideration.

Returning to the $n=0.5$ case, G_I evolutions present significant differences for $25^\circ \leq \theta_2 \leq 50^\circ$ with reference to the single-fibre case, both in the level of the curves and the position of their maxima, which occur when $\theta_d \approx \theta_2$. For $50^\circ \leq \theta_2 \leq 120^\circ$, G_I remains below the single-fibre case evolution, whereas for $130^\circ \leq \theta_2 \leq 155^\circ$ G_I stays above. In regards to the disappearance of G_I , it occurs for greater θ_d values than in the single-fibre case for $40^\circ \leq \theta_2 \leq 60^\circ$, all G_I evolutions vanishing for higher θ_d values than the uniaxial single-fibre case.

With reference to the G_{II} distributions, the maximum is reached at $\theta_d=70^\circ$ for the single-fibre case. Nevertheless, for $40^\circ \leq \theta_2 \leq 70^\circ$, the maximum takes places at a larger θ_d value than the single-fibre case and for $80^\circ \leq \theta_2 \leq 140^\circ$ the maximum occurs at a smaller θ_d value.

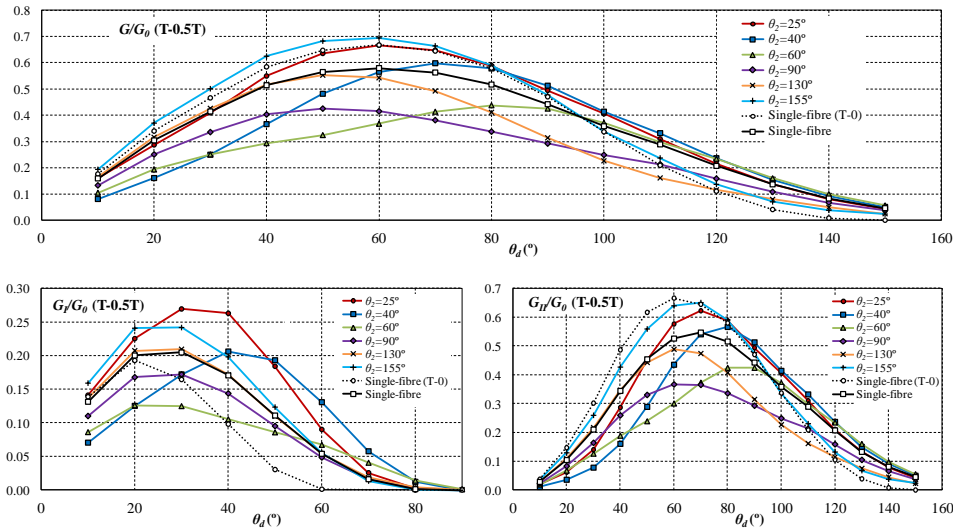


Figure 4. G/G_0 , G_I/G_0 and G_{II}/G_0 versus θ_d for $n=0.5$ and a selection of θ_2 values.

4. Propagation of the interface crack

The end of the unstable crack growth can be predicted as explained in [5], using the estimation of the critical value of the Energy Release Rate, G_c , based on [14], and comparing it with the corresponding G evolution:

$$G_c(\psi_k) = G_{Ic} [1 + \tan^2[(1-\lambda)\psi_k]] \quad (3)$$

where G_{Ic} is the critical value of G_c for Mode I and λ is the fracture mode sensitivity parameter (in this study, $\lambda=0.25$, a typical value for the bi-material system under consideration). ψ_k is the local phase angle and represents the evolution of the fracture mode mixity. It can be calculated following [15]. In the absence of direct experimental data, G_{Ic} has been adjusted as detailed in [5], making the G_c value associated with the first debond considered to coincide with the initial G value and establishing the uniaxial single-fibre G_{Ic} value as the reference for all the cases under consideration. As a consequence, all G evolutions start at the same G level, and therefore, a different level of load is needed to initiate the propagation for each case.

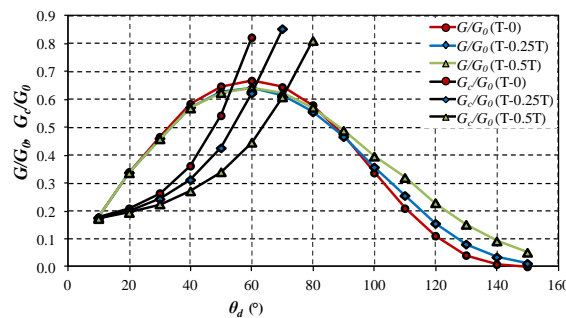


Figure 5. G/G_0 and G_c/G_0 versus θ_d for the single-fibre case and $n=0, 0.25, 0.5$

Fig. 5 shows the comparison between the G and G_c evolutions obtained for the single-fibre case and the biaxial cases corresponding to $n=0, 0.25, 0.5$. The $n \geq 0.5$ cases are not included in Fig. 5 for the sake of clarity and simplicity, these cases following the same tendency shown in the figure. The comparison between G and G_c determines a length of unstable growth of $\theta_d \approx 55^\circ$ for T-0, $\theta_d \approx 60^\circ$ for T-0.25T and $\theta_d \approx 70^\circ$ for T-0.5T, coinciding with the appearance of a finite size contact zone at the crack tip. Therefore, as the secondary load increases, the interface crack achieves greater lengths of unstable growth. This result was already found in [5].

The same approach is employed for the two-fibre case. Fig. 6 shows G and G_c evolutions for a selection of θ_2 values and the same biaxial cases. It is observed that, for $\theta_2=25^\circ$ and $\theta_2=40^\circ$ (Figs. 5a-b), there are not considerable differences between the lengths of unstable growth obtained for the biaxial cases under consideration ($\theta_d \approx 70^\circ$ and $\theta_d \approx 100^\circ$ respectively). Nevertheless, for $\theta_2=60^\circ$ and $\theta_2=80^\circ$ (Figs. 5c-d), as the secondary load increases, the unstable growth achieves greater debonding angles: for $\theta_2=60^\circ$ and $n=0, 0.25, 0.5$, the unstable growth stops at $\theta_d \approx 40^\circ$, $\theta_d \approx 55^\circ$ and $\theta_d \approx 90^\circ$, respectively, and for $\theta_2=80^\circ$ and $n=0, 0.25, 0.5$, $\theta_d \approx 50^\circ$, $\theta_d \approx 55^\circ$ and $\theta_d \approx 65^\circ$.

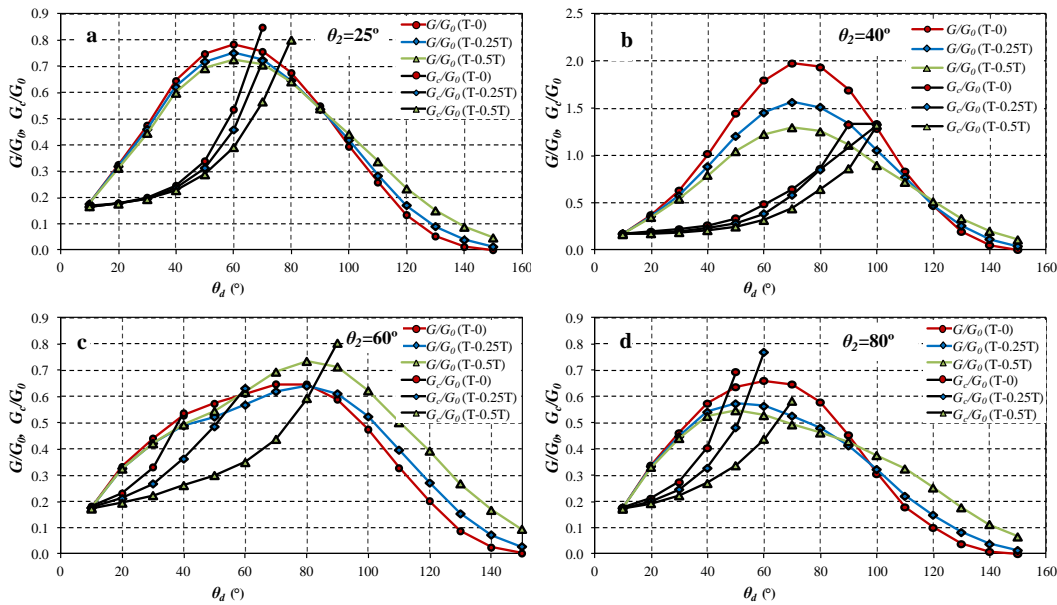


Figure 6. G/G_0 and G_c/G_0 versus θ_d for $n=0, 0.25, 0.5$: a) $\theta_2=25^\circ$, b) $\theta_2=40^\circ$, c) $\theta_2=60^\circ$, d) $\theta_2=80^\circ$.

Finally, to sum up and visualise the previous results, a scheme of the final deformed situation at the end of the unstable growth is represented in Fig. 7, both for the single-fibre case and a selection of θ_2 values, and for all biaxial cases taken under consideration in this study ($n=0, 0.25, 0.5, 0.75, 1$). For $n=0, 0.25$, the crack achieves greater lengths of unstable growth than the single-fibre case for the range $25^\circ \leq \theta_2 \leq 50^\circ$ and for $n=0.5$, the range of greater lengths of unstable growth is $25^\circ \leq \theta_2 \leq 60^\circ$. Nevertheless, this θ_2 range becomes wider as the level of the secondary load increases ($40^\circ \leq \theta_2 \leq 100^\circ$ for $n=0.75$ and $50^\circ \leq \theta_2 \leq 120^\circ$ for $n=1$). The positions where the lengths of unstable growth are smaller than those corresponding to the single-fibre case are $60^\circ \leq \theta_2 \leq 90^\circ$ for $n=0$, $60^\circ \leq \theta_2 \leq 80^\circ$ for $n=0.25$, $80^\circ \leq \theta_2 \leq 90^\circ$ for $n=0.5$, $\theta_2=130^\circ$ and $150^\circ \leq \theta_2 \leq 155^\circ$ for $n=0.75$ and $25^\circ \leq \theta_2 \leq 30^\circ$ and $140^\circ \leq \theta_2 \leq 155^\circ$ (positions aligned with the principal load) for $n=1$. Moreover, the end of the unstable growth is related to the appearance of a finite size contact zone at the crack tip for all cases under consideration, except for the positions $30^\circ \leq \theta_2 \leq 50^\circ$ for $n=0, 0.25$, since the crack stops growing after a considerable length of contact zone has been achieved.

It can also be observed in Fig.7 that, as the level of the secondary load increases, the lengths of unstable growth become larger but the differences between all θ_2 cases and their corresponding single-fibre case are smaller. This fact suggests that, as the level of the secondary load increases, the effects

produced by the biaxial loading predominate over the alterations provoked by the presence of the secondary fibre. This issue is similar to that previously observed in Section 3 in relation to the differences between the level of G evolutions with reference to the single-fibre case.

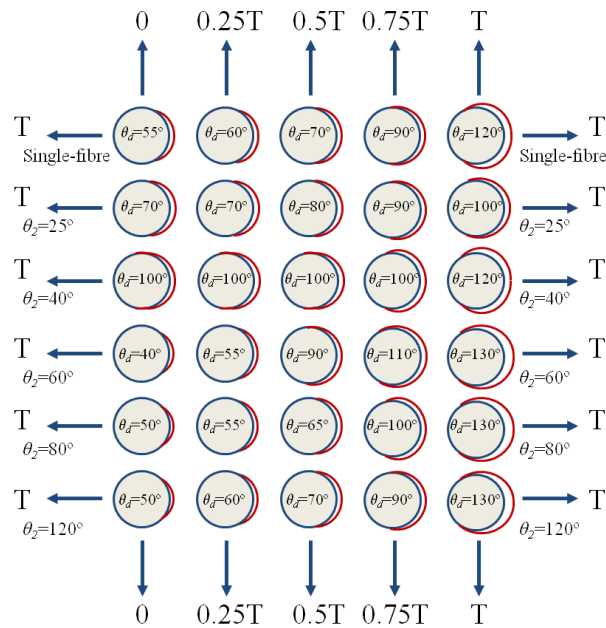


Figure 7. Scheme of the final deformed situation at the end of the unstable growth.

5. Effect of the distance between the fibres

The variation of the distance between the fibres allows an r_2 value, from which the influence of the secondary fibre could be ignored, to be established. For that purpose, the analysis carried out in the previous sections is implemented for increasing values of r_2 . The results presented in [6] for the uniaxial tensile case established that the effects of the presence of the secondary fibre remained until the ratio $r_2/r_2^0=7$ was achieved. Nevertheless, the results obtained with the present two-fibre model show that, as the level of the secondary load increases, the distance needed to ignore the effects produced by the secondary fibre decreases. In particular, for $n=0.5$, this ratio decreases until $r_2/r_2^0=5$ and finally, it decreases until $r_2/r_2^0=3$ for $n=1$.

6. Conclusions

With regard to the propagation of the interface crack, it is observed that, as the secondary load increases: 1) the end of the unstable growth is produced at greater debonding angles for a fixed θ_2 value (this effect was already detected by the authors for uniaxial tension in [5]); 2) the differences between the θ_2 cases and their corresponding single-fibre case become smaller, and 3) the θ_2 ranges for which the length of unstable growth is greater than its corresponding single-fibre case are wider.

According to the initial G value, when the secondary load is lower than or equal to the principal load ($n=0.25, 0.5$), the presence of the nearby fibre (for most of its positions) intensifies the inhibition of the mechanism of failure observed in the single-fibre case for biaxial tensile loads [5]. This tendency is not maintained when the nearby fibre is approximately aligned with the direction of the principal load, the presence of the fibre involving an accelerative effect versus failure. For higher levels of the secondary load ($n=0.75, 1$), the undamaged fibre reverses this accelerative effect and maintains the protective effect due to the biaxial tensile loads (previously observed with reference to the single-fibre case) for all relative positions between the two fibres.

With reference to the distance between the fibres, the total disappearance of the effects produced by the presence of the secondary fibre is achieved at $r_2/r_2^0=7$, $r_2/r_2^0=5$ and $r_2/r_2^0=3$ for $n=0, 0.5, 1$ respectively. Consequently, as the level of the secondary load increases, the distance needed to ignore the alterations brought about by the undamaged fibre decreases considerably.

On a final note, it is important to remark that the results obtained with the two-fibre model (in relation to the evolution of the Energy Release Rate, the propagation of the interface crack and the influence of the distance between the fibres) suggest that, as the level of the secondary load increases, the effects of the biaxial loading predominate over the alterations brought about by the presence of the undamaged secondary fibre, with reference to the uniaxial single-fibre case.

Acknowledgements

This study was supported by the Spanish Ministry for Education and Science/Economy and Competitiveness and the Junta de Andalucía (Projects MAT2013-45069-P, DPI 2012-37187 and P11-TEP-7093). The authors would like to thank Dr. E. Graciani (University of Seville) whose BEM code was used.

References

- [1] F. París, E. Correa and V. Mantič. Kinking of transverse interface cracks between fibre and matrix. *J App Mech*, 74: 703–716, 2007.
- [2] F. París, E. Correa and J. Cañas. Micromechanical view of failure of the matrix in fibrous composite materials. *Compos Sci Technol*, 63: 1041–1052, 2003.
- [3] E. Correa, E.K. Gamstedt, F. París and V. Mantič. Effects of the presence of compression in transverse cyclic loading on fibre–matrix debonding in unidirectional composite plies. *Composites Part A*, 38: 2260–2269, 2007.
- [4] E. Correa, V. Mantič and F. París. Effect of thermal residual stresses on the matrix failure under transverse tension at micromechanical level. A numerical and experimental analysis. *Compos Sci Technol*, 71(5): 622–629, 2011.
- [5] E. Correa, F. París and V. Mantič. Effect of the presence of a secondary transverse load on the inter-fibre failure under tension. *Eng Fract Mech*, 103: 174–189, 2013.
- [6] C. Sandino, E. Correa, F. París. Numerical analysis of the influence of a nearby fibre on the interface crack growth in composites under transverse tensile load. *Engng Fract Mech*. 2016.
- [7] C. Sandino, E. Correa, F. París. Study of the influence of a nearby fibre on the interface crack growth under transverse compression. *XI Spanish National Congress on Composite Materials, Móstoles, Spain*, July 6-8 2015.
- [8] V. Mantič, A. Blázquez, E. Correa and F. París. Analysis of interface cracks with contact in composites by 2D BEM. In M. Guagliano and M.H. Aliabadi, editors. *Fracture and Damage of Composites*, pages 189–248. WIT Press, Southampton, 2006.
- [9] F. París and J. Cañas. *Boundary Element Method. Fundamentals and Applications*. OUP, Oxford, 1997.
- [10] E. Graciani. *Formulation and implementation of BEM for axisymmetric problems with contact. Application to characterization of the fibre–matrix interface in composites*. PhD thesis, University of Seville, 2006.
- [11] G.R. Irwin. Analysis of stresses and strain near the end of a crack transversing a plate. *J App Mech*, 24: 361–364, 1957.
- [12] M. Toya. A crack along the interface of a circular inclusion embedded in an infinite solid. *J Mech Phys Solids*, 22: 325–348, 1974.
- [13] Y. Murakami. *Stress Intensity Factor Handbook*. Pergamon Press, Oxford, 1988.
- [14] J.W. Hutchinson and Z. Suo. Mixed mode cracking in layered materials. *Adv App Mech*, 29: 63–191, 1992.
- [15] V. Mantič and F. París. Relation between SIF and ERR based measures of fracture mode mixity in interface cracks. *Int. J. Fracture*, 130: 557–569, 2004.